JPE 17-2-1

https://doi.org/10.6113/JPE.2017.17.2.315
ISSN(Print): 1598-2092 / ISSN(Online): 2093-4718

An E-capless AC-DC CRM Flyback LED Driver with Variable On-time Control

Kai Yao†, Xiaopeng Bi*, and Siwen Yang*

†,*School of Automation, Nanjing University of Science and Technology, Nanjing, China

Abstract

LED is a promising new generation of green lighting with the advantages of high efficiency, good optical performance, long lifetime and environmental friendliness. A pulsating current can be used to drive LEDs. However, current with a high peak-to-average ratio is unfavorable for LEDs. A novel control scheme for the ac-dc critical conduction mode (CRM) flyback LED driver is proposed in this paper. By using the input voltage, output voltage and average output current to control the turn-on time of the switch, the peak-to-average ratio of the output current can be reduced. The operation principle is analyzed and an implementation circuit is put forward. Experimental results show the effectiveness of the proposed scheme.

Key words: CRM, Flyback converter, LED, Peak-to-average ratio

I. INTRODUCTION

Compared to conventional fluorescent lamps, high brightness light-emitting diodes (HB-LEDs) have many excellent characteristics, including high efficiency, long lifetime, compact size, high brightness, rich color, and very low maintenance cost [1], [2].

For high-power HB-LED drivers, power factor correction (PFC) must be imposed to achieve a high power factor (PF) and low input current harmonics to meet relevant harmonics standard such as IEC 61000-3-2 [3] and Energy Star [4].

Regardless of the types of AC–DC converter, in order to achieve power decoupling between the ac input power and the constant dc output power, the storage capacitors used in AC–DC converters have to have a larger capacitance. Compared with other types of capacitor, electrolytic capacitors have a higher capacitance and energy density. Thus, electrolytic capacitors are mostly chosen in AC–DC converters. The lifetime of an electrolytic capacitor (E-cap) is about 5000 hours [5]. On the other hand, the estimated useful lifetime of LEDs is about 50000 h [6]. In order to extend the expected lifetime of LED drivers, the E-cap should be removed from the circuit. The methods for achieving this can be approximately divided into the five types that follow. The first type is adopting energy storage elements to handle the instantaneous input and output power difference [7]-[9]. The second type is working on the control loop of the converters in order to lower the output current ripple without the need for increasing the capacitor size [10], [11]. The third type is using a relatively new approach in which the majority of the input power reaches the LEDs through one stage of conversion while the rest of the power is processed in some other stages after passing the first stage toward the LEDs [12].

The methods mentioned above aim to obtain a constant current to drive LEDs. In addition to constant current, pulsating current can also be used to drive LEDs [13], [14]. According to the experimental investigation in [15], as shown in Fig. 1, the flux of the LEDs is approximately proportional to the average value of the output current and is independent of its frequency.

Although pulsating current can be used to drive a LED, and its brightness can be regulated by regulating the average current, the peak-to-average ratio of the driving current should be limited to avoid overdriving. Unless this is done, the LED will be damaged. According to the technical datasheets [16] and [17], and the experimental investigation in [18], each LED has a maximum tolerable current, and it decreases as the operating temperature increases. If the peak-to-average ratio of the driving current is too high, the average driving current to be delivered to the LED should be reduced to avoid damage. However, this leads to poor utilization of the LED.

Manuscript received May 25, 2016; accepted Nov. 25, 2016
Recommended for publication by Associate Editor Chun-An Cheng.
†Corresponding Author: yaokai@njust.edu.cn
Tel/Fax: +86-25-84315468, Nanjing University of Science and Technology
*School of Automation, Nanjing University of Science and Technology, China

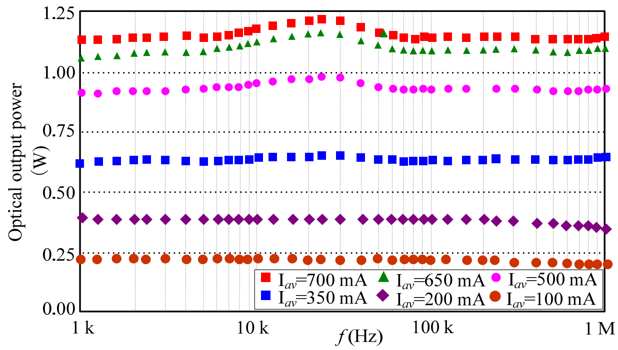

Fig. 1. Optical variation of high-brightness LEDs driven by pulsating current.

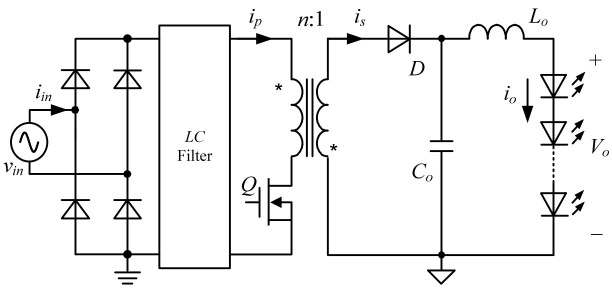

Fig. 2. Main circuit of the flyback LED driver without electrolytic capacitor.

The objective of this paper is to propose an electrolytic capacitor-less ac–dc LED driver, which converts commercial ac voltage into a pulsating current with twice the line frequency to drive high-brightness LEDs. Section II presents the concept of an electrolytic capacitor-less ac–dc driver for LED lighting. In addition, the operation principle of a CRM flyback converter with constant on-time control for a LED driver is analyzed. The concept and implementation circuit of a variable on-time control to reduce the peak-to-average ratio of the output current are presented in Section III. In Section IV, a performance comparison is made in terms of the design of the inductor, the switching frequency, the peak and rms value of the inductor current, and the conduction and turn-off losses of the switch. Experimental results from a 48 V, 0.7 A output prototype are presented in Section V. Finally, some conclusions are presented in Section VI.

II. Operation Principle of an E-cap-less AC-DC CRM Flyback LED Driver

Fig. 2 shows the main circuit of the proposed flyback LED driver.

The input voltage is defined as:

$$v_{in} = V_m \sin \omega t = V_m \sin 2\pi f_l t \tag{1}$$

where V_m, ω, and f_l are the amplitude, angular frequency and line frequency of the input voltage, respectively.

Then the rectified voltage is:

$$v_g = V_m \left|\sin \omega t\right| \tag{2}$$

Fig. 3 shows inductor current waveforms of the switching cycles where the converter operates in the CRM. In a switching cycle, the peak current of the primary inductor is:

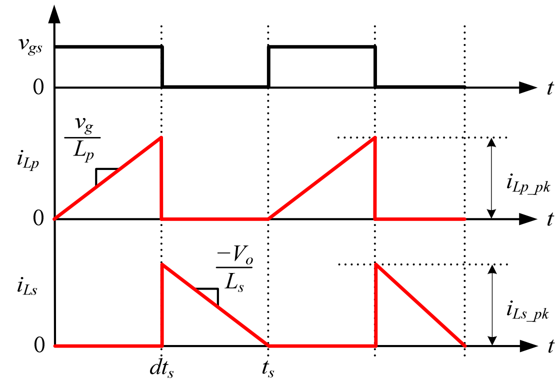

Fig. 3. Inductor current waveforms in switching cycles.

$$i_{Lp\_pk} = \frac{V_m \left|\sin \omega t\right|}{L_p} t_{on} \tag{3}$$

where L_p is the primary inductance, and t_{on} is the on-time of the switch in a switching cycle.

Then the off-time of the switch is:

$$t_{off} = \frac{i_{Ls\_pk}}{V_o/L_s} = \frac{n i_{Lp\_pk}}{n^2 V_o/L_p} = \frac{V_m \left|\sin \omega t\right|}{n V_o} t_{on} \tag{4}$$

where L_s is the secondary inductance, n is the turns ratio of the inductor, and V_o is the output voltage.

From (4), the duty cycle is derived as:

$$d = \frac{t_{on}}{t_s} = \frac{t_{on}}{t_{on} + t_{off}} = \frac{n V_o}{n V_o + V_m \left|\sin \omega t\right|} \tag{5}$$

The average value of the primary inductor current in a switching cycle is:

$$i_{Lp\_av} = \frac{1}{2} i_{Lp\_pk} d(t) = \frac{n V_o V_m \left|\sin \omega t\right|}{2L_p \left(n V_o + V_m \left|\sin \omega t\right|\right)} t_{on} \tag{6}$$

Therefore, the input current is:

$$i_{in} = \frac{n V_o V_m \sin \omega t}{2L_p \left(n V_o + V_m \left|\sin \omega t\right|\right)} t_{on} \tag{7}$$

From (1) and (7), the average input power is:

$$P_{in} = \frac{1}{\pi} \int_0^{\pi} v_{in} i_{in} d\omega t = \frac{1}{\pi} \int_0^{\pi} \frac{t_{on} n V_o \left(V_m \sin \omega t\right)^2}{2L_p \left(n V_o + V_m \left|\sin \omega t\right|\right)} d\omega t \tag{8}$$

Generally, for the purpose of a simple realization, t_{on} is constant in a line cycle. This is called COT control. Assuming that the efficiency of the converter is 100%, i.e., P_{in}=P_o, then the on-time of the switch is:

$$t_{on} = \frac{2\pi L_p P_o}{n V_o V_m^2 \int_0^{\pi} \frac{\left(\sin \omega t\right)^2}{n V_o + V_m \left|\sin \omega t\right|} d\omega t} \tag{9}$$

The substitution of (9) into (7) leads to:

$$i_{in} = \frac{\pi P_o \sin \omega t}{V_m \left(n V_o + V_m \left|\sin \omega t\right|\right)} \frac{1}{\int_0^{\pi} \frac{\left(\sin \omega t\right)^2}{n V_o + V_m \left|\sin \omega t\right|} d\omega t} \tag{10}$$

From (1) and (10), the input power factor is derived as:

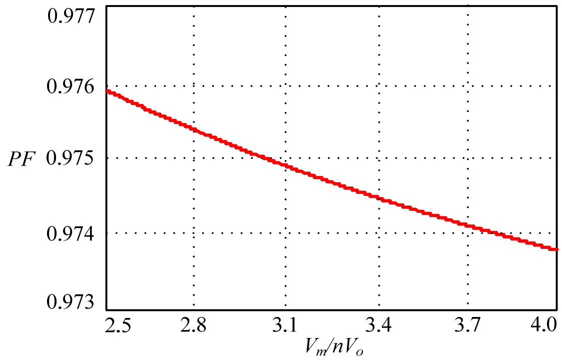

Fig. 4. Relationship between PF and V_m/nV_o.

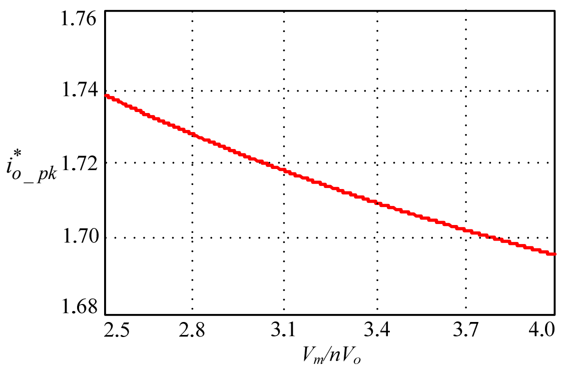

Fig. 5. Relationship between the peak-to-average ratio of the output current and V_m/nV_o.

$$PF = \frac{P_{in}}{\frac{1}{\sqrt{2}}V_m I_{in\_rms}} = \frac{\sqrt{\frac{2}{\pi}}\int_0^\pi \frac{(\sin\omega t)^2}{1+\frac{V_m}{nV_o}|\sin\omega t|}d\omega t}{\sqrt{\int_0^\pi \left(\frac{\sin\omega t}{1+\frac{V_m}{nV_o}|\sin\omega t|}\right)^2 d\omega t}} \tag{11}$$

Fig. 4 can be plotted according to (11) and the specifications given in section V, which shows that the PF decreases slightly when the input voltage increases.

According to the power balance, the average value of the secondary inductor current in a switching cycle is:

$$i_o = \frac{v_{in}i_{in}}{V_o} = \frac{\pi P_o(\sin\omega t)^2}{V_o(nV_o+V_m|\sin\omega t|)\int_0^\pi \frac{(\sin\omega t)^2}{nV_o+V_m|\sin\omega t|}d\omega t} \tag{12}$$

The peak-to-average ratio of the output current can be deduced from (12) as:

$$i^*_{o\_pk} = \frac{i_{o\_pk}}{I_o} = \frac{\pi}{(nV_o+V_m)\int_0^\pi \frac{(\sin\omega t)^2}{nV_o+V_m|\sin\omega t|}d\omega t} \tag{13}$$

Fig. 5 can be plotted from (13). As can be seen, the peak-to-average ratio is high over the input voltage range.

L_o and C_o are used to filter the high-frequency harmonics in the secondary current. The attenuation ratio of the current harmonic is:

$$\xi = \left|\frac{I_o(j\omega)}{I_s(j\omega)}\right| = \left|\frac{\frac{1}{j\omega C_o}}{\frac{1}{j\omega C_o}+j\omega L_o}\right| = \left|\frac{1}{1-L_oC_o\omega^2}\right| \tag{14}$$

For better attenuation, ξ should be as small as possible. However, a smaller ξ requires a larger L_oC_o, which means a larger filter size. Here, ξ=0.05 is selected at a switching frequency of 30 kHz. Substituting these values into (14) leads to L_oC_o=591×10^{-12}, and L_o=126μH and C_o=4.7μF are selected when ceramic capacitors can be adopted.

III. Variable On-time Control to Reduce Peak-to-average Ratio of the Output Current

By a Fourier analysis, the fundamental component amplitude of the input current shown in (10) is:

$$I_1 = \frac{2}{\pi}\int_0^\pi i_{in}\cdot\sin\omega t d\omega t$$
$$= \frac{2}{\pi}\int_0^\pi \frac{\frac{\pi P_o}{V_m}\cdot\frac{\sin\omega t}{nV_o+V_m|\sin\omega t|}}{\int_0^\pi \frac{(\sin\omega t)^2}{nV_o+V_m|\sin\omega t|}d\omega t}\cdot\sin\omega t d\omega t = \frac{2P_o}{V_m} \tag{15}$$

Therefore, the fundamental input current is:

$$i_1 = \frac{2P_o}{V_m}\sin\omega t \tag{16}$$

The output current generated by this fundamental component is:

$$i_o = \frac{V_m\sin\omega t\cdot\frac{2P_o}{V_m}\sin\omega t}{V_o} = \frac{2P_o}{V_o}(\sin\omega t)^2 \tag{17}$$

(16) and (17) show that if the power factor is unity, the peak-to-average ratio of the output current is 2, which is relatively high. Therefore, there is a tradeoff between the power factor and the peak-to-average ratio of the output current, which is similar to the analysis in [19]. In order to realize a lower peak-to-average ratio, the input voltage is introduced into the variation of the input current.

$$i'_{in} = \frac{2P_o}{V_m}\sin\omega t\cdot a(1-k|\sin\omega t|) \tag{18}$$

where k is a coefficient representing the degree of the introduced input voltage, and a is a function of k. As a result, the average output current can be reached.

Based on (7) and (18), the required t_{on} to generate the desired input current is:

$$t'_{on} = \frac{4P_oL_p(nV_o+V_m|\sin\omega t|)}{nV_oV_m^2}a(1-k|\sin\omega t|) \quad a>0,\ 0<k<1 \tag{19}$$

It can be seen from (19) that the on-time of the switch is variable with the input voltage. This is referred to as variable on-time (VOT) control.

From (1) and (18), the output current is:

$$i'_o = \frac{v_{in}i'_{in}}{V_o} = \frac{2aP_o}{V_o}(\sin\omega t)^2(1-k|\sin\omega t|) \tag{20}$$

Ensure that the average value of (20) in a half line cycle is equal to I_o, then:

$$a=\frac{3\pi}{3\pi-8k} \tag{21}$$

From (1), (18) and (21), the power factor with the VOT control is:

$$PF=\frac{P_{in}}{\frac{1}{\sqrt{2}}V_m I'_{in\_rms}}=\frac{\frac{\sqrt{\pi}}{\sqrt{2}}\left(1-\frac{8}{3\pi}k\right)}{\sqrt{\frac{\pi}{2}-\frac{8}{3}k+\frac{3\pi}{8}k^2}} \tag{22}$$

Ensure that the input power factor is higher than 0.9 to meet regulatory requirements such as the ENERGY STAR. Solving (18) leads to $0<k<0.831$.

With the base of I_o, the normalized output current is:

$$i'^{*}_{o}=\frac{6\pi(\sin\omega t)^2(1-k|\sin\omega t|)}{3\pi-8k} \tag{23}$$

(23) is a function of ωt and its maximum is the peak-to-average ratio of the output current. It is also noted that the shape of (23) is symmetrical about $\omega t=\pi/2$. Differentiating (23) with ωt and setting it equal zero yields:

$$\left(1-\frac{3}{2}k\sin\omega t\right)\sin\omega t\cos\omega t=0 \tag{24}$$

It can be seen from (24) that, ωt=0, π/2, π with $0<k<2/3$ and ωt=0, arcsin2/3k, π/2, π-arcsin2/3k, π with $2/3<k<0.831$ can be obtained. Then the peak-to-average ratio of the output current is:

$$i'^{*}_{o\_pk}=\begin{cases}\dfrac{6\pi(1-k)}{3\pi-8k} & 0<k<2/3\\[2ex] \dfrac{8\pi}{9k^2(3\pi-8k)} & 2/3<k<0.831\end{cases} \tag{25}$$

When k=π/4, the minimum value of 1.44 is obtained from (25). Substituting k=π/4 into (21) and (22) results in a = 3 and PF = 0.927.

According to the datasheet of the L6561, the control circuit can be implemented as shown in Fig. 6. Proper selection of the resistances can enable the voltage of point G as follows:

$$v_G=v_{EA}\cdot k_{vg}V_m|\sin\omega t| \tag{26a}$$

$$v'_G=v_{EA}\cdot k_{vg}^3V_m^2|\sin\omega t|\left(nV_o+V_m|\sin\omega t|\right)\left(1-0.785|\sin\omega t|\right) \tag{26b}$$

where k_{vg} is the sensor gain of the rectified input voltage and output voltage.

The current of the flyback switch is sensed through the series resistor R_s, and v_{Rs} is obtained. v_G and v_{Rs} are connected to the comparator. The output of comparator and the ZCD is connected to the reset pin and set pin of the RS trigger, which drives the flyback switch to work.

When the switch is on, the voltage across the current sensor resistor is:

$$v_{Rs}=\frac{V_m|\sin\omega t|}{L_p}t_{on}R_s \tag{27a}$$

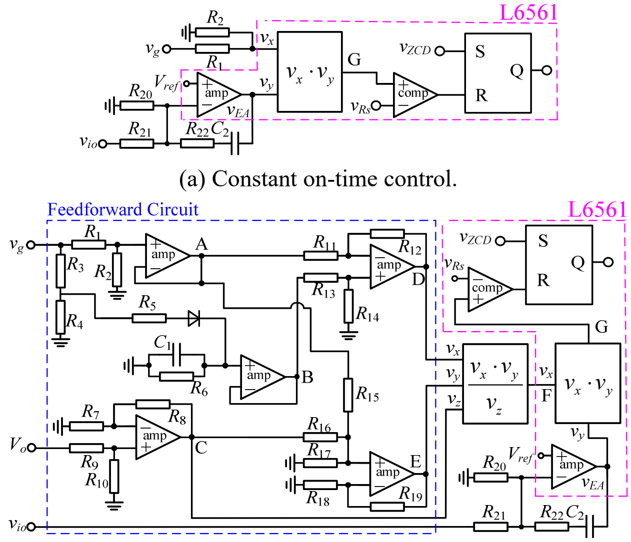

(a) Constant on-time control.

(b) Variable on-time control.

Fig. 6. Control circuit of the converter.

$$v'_{Rs}=\frac{V_m|\sin\omega t|}{L'_p}t'_{on}R_s \tag{27b}$$

v_{Rs} increases with the current and when it reaches the value of v_G expressed in (26), and the switch will turn off. The on-time of the switch is obtained by combining (26) and (27):

$$t_{on}=\frac{k_{vg}v_{EA}L_p}{R_s} \tag{28a}$$

$$t'_{on}=\frac{k_{vg}^3v_{EA}L'_pV_m\left(nV_o+V_m|\sin\omega t|\right)\left(1-0.785|\sin\omega t|\right)}{R_s} \tag{28b}$$

Obviously, (28a) and (28b) are in the same form as (9) and (19). Therefore, the desired constant on-time control and variable on-time control are realized.

IV. Performance Comparison

A. The Switching Frequency and Inductor's Ripple Current

From (4), (9) and (19), the switching frequency with the COT and VOT control can be derived as:

$$f_s=\frac{1}{t_{on}+t_{off}}=\frac{(nV_oV_m)^2\int_0^{\pi}\frac{(\sin\omega t)^2}{nV_o+V_m|\sin\omega t|}d\omega t}{2\pi L_pP_o\left(nV_o+V_m|\sin\omega t|\right)} \tag{29a}$$

$$f'_s=\frac{(nV_oV_m)^2}{12L'_pP_o\left(nV_o+V_m|\sin\omega t|\right)^2\left(1-0.785|\sin\omega t|\right)} \tag{29b}$$

At a certain input voltage, there is a minimum value during a half line cycle of [0, π] for (29a) and (29b), respectively. Considering the human hearing frequency range, the minimum switching frequency is set to f_{s_min}=30kHz. Based on the specifications of the converter, the relationship between the required critical inductance and the input voltage

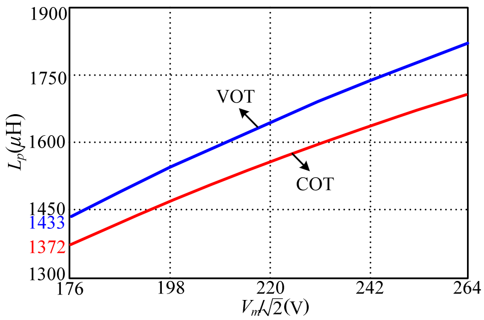

Fig. 7. Critical inductance over the input voltage.

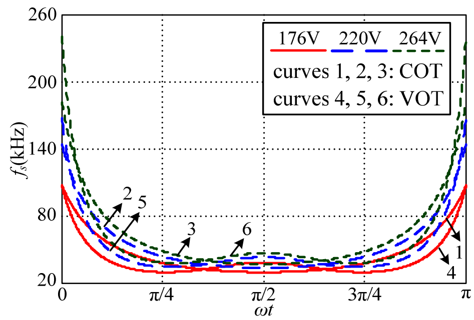

Fig. 8. Switching frequency in half a line cycle.

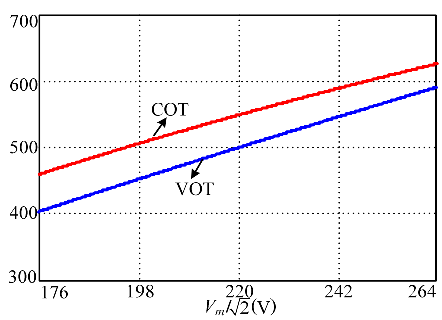

Fig. 9. Number of switching times in half a line cycle.

can be deduced from (29a) and (29b), which is depicted in Fig. 7. It can be seen that the inductances are 1372μH and 1433μH, for the COT and VOT controls, respectively. Therefore, the switching frequency curves of the converter in a half line cycle can be plotted, as shown in Fig. 8. It can be seen that, around 0, π/2 and π of a certain input voltage, the switching frequency with the VOT control is higher than that with the COT control. Meanwhile, around π/8 and π7/8, the opposite is the true.

The total number of the switching times in half a line cycle can be derived as:

$$\int_0^{T_l/2} f_s(t)dt = \frac{1}{\omega}\int_0^{\pi} f_s(\omega t)\,d\omega t \tag{30}$$

Fig. 9 can be drawn based on (29-30). The VOT control achieves a switching number reduction of 12.1% and 5.6% at 176 VAC and 264 VAC, respectively.

According to (3), (9) and (19), the peak current of the primary inductor with the COT and VOT control can be obtained as:

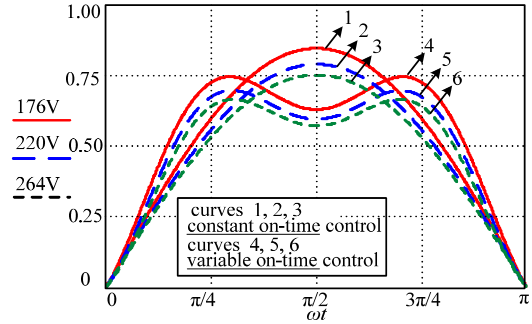

Fig. 10. Peak current of the primary inductor in half a line cycle.

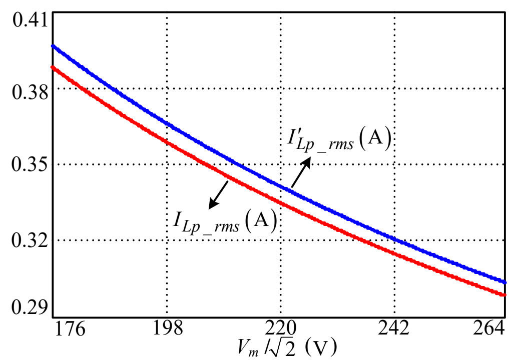

Fig. 11. Rms value of the primary inductor current.

$$i_{Lp\_pk} = \frac{2\pi P_o|\sin\omega t|}{nV_oV_m\int_0^{\pi}\frac{(\sin\omega t)^2}{nV_o+V_m|\sin\omega t|}d\omega t} \tag{31a}$$

$$i'_{Lp\_pk} = \frac{12P_o}{nV_mV_o}|\sin\omega t|(nV_o+V_m|\sin\omega t|)(1-0.785|\sin\omega t|) \tag{31b}$$

(31) can be plotted in Fig. 10. As can be seen, with variable on-time control, the peak current of the switch decreases around π/2 and increases around π/4 and 3π/4.

In a switching cycle, the rms value of the primary inductor current is:

$$i_{Lp\_rms} = \sqrt{\frac{1}{t_s}\cdot\int_0^{t_{on}}\left(\frac{v_g}{L_p}\cdot t\right)^2\cdot dt} = \frac{V_m|\sin\omega t|}{L_p}\sqrt{\frac{t_{on}^3}{3t_s}} \tag{32a}$$

$$i'_{Lp\_rms} = \sqrt{\frac{1}{t'_s}\cdot\int_0^{t'_{on}}\left(\frac{v_g}{L'_p}\cdot t\right)^2\cdot dt} = \frac{V_m|\sin\omega t|}{L'_p}\sqrt{\frac{t'^3_{on}}{3t'_s}} \tag{32b}$$

Furthermore, from (9), (19) and (32), the rms value in half a line cycle can be obtained as:

$$I_{Lp\_rms} = \sqrt{\frac{1}{\pi}\int_0^{\pi} i_{Lp\_rms}^2 d\omega t} = \frac{2P_o}{V_m}\sqrt{\frac{\pi}{3nV_o\int_0^{\pi}\frac{(\sin\omega t)^2}{nV_o+V_m|\sin\omega t|}d\omega t}} \tag{33a}$$

$$I'_{Lp\_rms} = \frac{4P_o}{V_m}\sqrt{\frac{3}{nV_o\pi}\int_0^{\pi}\sin^2\omega t(1-0.785|\sin\omega t|)^2(nV_o+V_m|\sin\omega t|)d\omega t} \tag{33b}$$

Fig. 11 is drawn based on (33). It can be seen that the VOT control brings about a small increment of the rms value.

The primary and secondary turns numbers N_p and N_s, the section area of the winding S, the air gap δ, and the filling factor K_u of the inductor are:

$$N_p = \frac{L_{p\_max} I_{Lp\_pk\_max}}{\Delta B A_e} \tag{34a}$$

$$N_s = \frac{N_p}{n} \tag{34b}$$

$$S_1 = \frac{I_{Lp\_rms\_max}}{J} \tag{35a}$$

$$S_2 = \frac{I_{Ls\_rms\_max}}{J} \tag{35b}$$

$$\delta = \frac{\mu_0 N_p^2 A_e}{L_p} \tag{36}$$

$$K_\mu = \frac{N_p S_1 + N_s S_2}{A_w} \tag{37}$$

where $I_{Lp\_pk\_max}$ is the maximum value of the primary inductor's peak current, ΔB is the flux density, A_e and A_w are the effective and window area of the magnetic core, $I_{Lp\_rms\_max}$ and $I_{Ls\_rms\_max}$ are the maximum values of the primary and secondary inductor's rms current, J is the current density, and μ_0 is the permeability.

Substituting L_{p_max}, $I_{Lp\_pk\_max}$, $I_{Lp\_rms\_max}$ and L'_{p_max}, $I'_{Ls\_pk\_max}$, $I'_{Ls\_rms\_max}$ into (36) and (37), δ and K_μ for the COT and VOT control can be calculated, and the results are nearly the same. This means that the inductor remains basically the same.

B. Conduction and Turn-Off Loss of the Switch

The conduction loss of the switch is:

$$P_{Qb\_con} = I_{Qb\_rms}^2 R_{ds\_on} = \frac{R_{ds\_on}}{3\pi} \int_0^\pi i_{p\_pk}^2(t) \frac{t_{on}}{t_s} d\omega t \tag{38}$$

A SSS5N80A is selected as the switch, whose conduction resistance R_{ds_on}=2.2Ω. Substituting (5) and (31) into (38), and combining the specifications of the converter, the conduction losses for the COT and VOT control are obtained.

Due to the CRM, the switch features zero-current turn-on. The turn off loss in a switching cycle can be derived as:

$$p_{Q\_off} = \frac{1}{2}\left(V_m |\sin\theta| + V_o\right) i_{Lp\_pk} t_f f_s \tag{39}$$

Then, the turn off loss in a line cycle is:

$$P_{Q\_off} = \frac{1}{\pi}\int_0^\pi \frac{1}{2}\left(V_m |\sin\theta| + V_o\right) i_{Lp\_pk} t_f f_s \, d\omega t \tag{40}$$

Substituting (29) and (31) into (40), the switching off loss for the COT and VOT control are obtained, as shown in Fig. 12.

It is clear that the VOT control achieves a small reduction of the turn off loss and a slight increase of the conduction loss.

V. EXPERIMENTAL VERIFICATION

A prototype has been built and tested in the laboratory, as shown in Fig. 13. The specifications and main components are as follows: input voltage: v_{in}=176~264 VAC/50Hz; output voltage: V_o=48 VDC; output current: I_o=0.7 A; switching frequency: f_s≥30 kHz; bridge rectifier: GBL206; power switch: SSS5N80A; output diode: MUR550; magnetic core: RM14; and control IC: L6561.

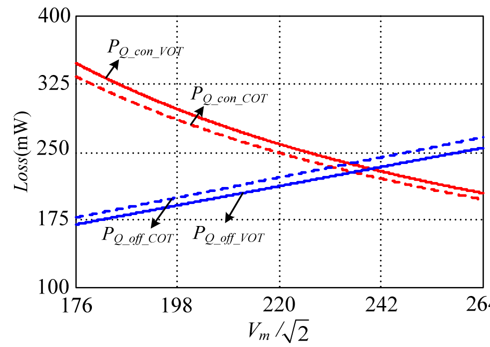

Fig. 12. Conduction loss and turn-off loss of the switch.

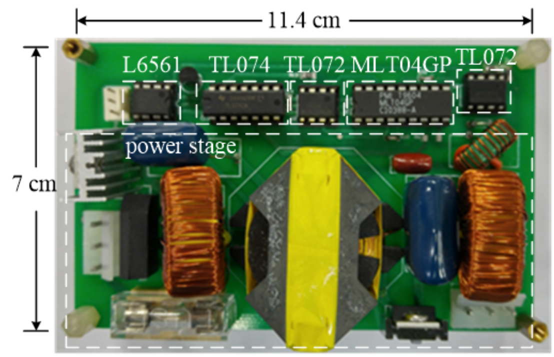

Fig. 13. Photo of the prototype.

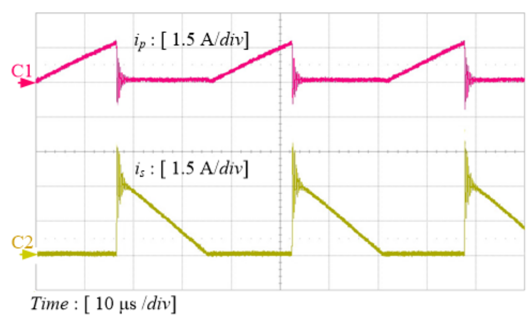

Fig. 14. Experimental waveforms of i_p and i_s.

Fig. 14 shows waveforms of the primary and secondary current at a normal input voltage of 220 VAC. It can be seen that the flyback converter operates in the CRM.

Fig. 15 shows experimental waveforms at a normal input voltage of 220 VAC. The measured average values of the output current are both 0.695, and the measured peak values are 1.193A and 1.015A, for the COT and VOT controls, respectively. This means that the peak-to-average ratio of the output current decreases from 1.72 to 1.46, which is in good agreement with that of the theoretical analysis.

The measured power factor is plotted in Fig. 16. It shows that, in the whole input voltage range, for the converter with the VOT control, the power factor is about 0.92, which is lower than that with the COT control. The measured value is in accordance with the theoretical one.

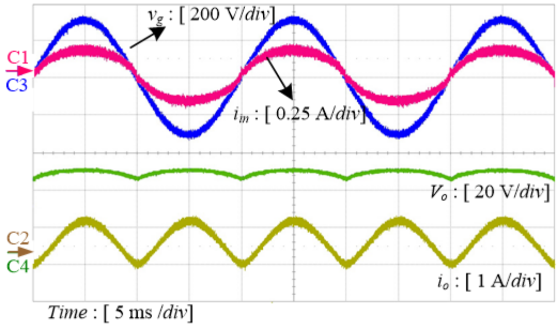

(a) Constant on-time control

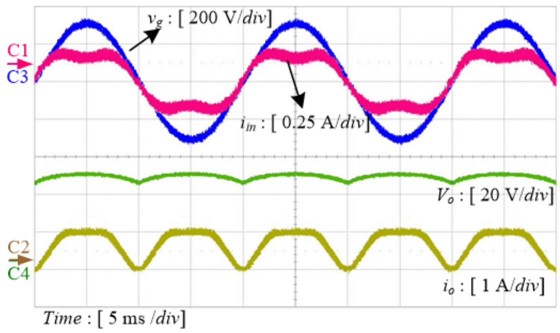

(b) Variable on-time control

Fig. 15. Experimental waveforms of the input voltage, input current, output voltage, and output current.

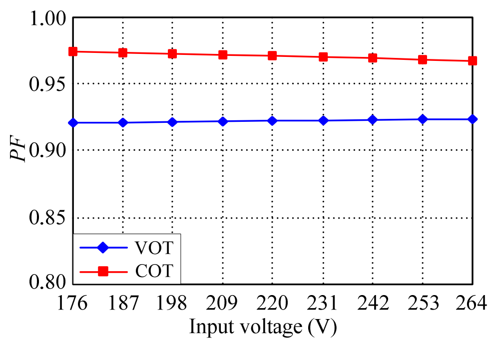

Fig. 16. Measured power factor.

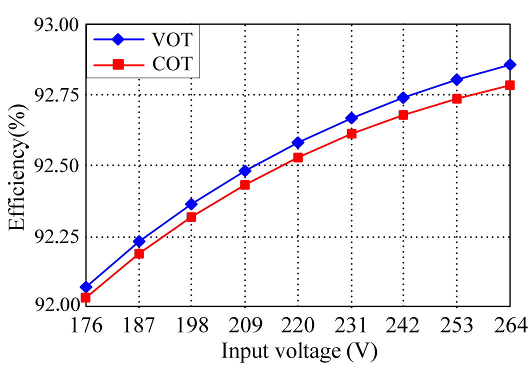

Fig. 17. Measured efficiency.

Compared to that with the COT control, the measured efficiency of the converter with the VOT control is slightly higher, which is shown in Fig. 17.

The standard limits of IEC61000-3-2 Class D and the measured input current harmonics of the converter with the VOT control are illustrated in Table I. It can be seen that the harmonics satisfy the criteria very well.

TABLE I
MEASURED INPUT CURRENT HARMONICS

	$\frac{I_3}{P_{in}}$	$\frac{I_5}{P_{in}}$	$\frac{I_7}{P_{in}}$	$\frac{I_9}{P_{in}}$	$\frac{I_{11}}{P_{in}}$	$\frac{I_{13}}{P_{in}}$
Input current harmonics (mA/W)	1.941	0.273	0.091	0.042	0.023	0.014
IEC61000-3-2 Class D (mA/W)	3.4	1.9	1.0	0.5	0.35	0.296

VI. CONCLUSIONS

In this paper, an electrolytic capacitor-less ac-dc flyback LED driver is proposed, which converts commercial ac voltage into a pulsating current to drive LEDs. In this way, the electrolytic capacitor can be thoroughly removed. Further, a variable on-time control and an implementation circuit are put forward to reduce the peak-to-average ratio of the output current to a minimum. The design of the inductor, the switching frequency, the peak and rms value of the inductor current, the conduction and turn-off losses of the switch are analyzed. The advantage of the method is that no additional power components need to be added in the main circuit. The disadvantage is that the power factor and THD are not high. However, in spite of this, the input current harmonics still meet the ENERGY STAR and IEC61000-3-2 Class D standard. Experimental results show the validity of the proposed scheme.

ACKNOWLEDGMENT

This work was supported by the national natural science foundation of China (51307085, 51677091), excellent youth fund project of Jiangsu natural science foundation (BK20160086), six talents peak project of Jiangsu (XNY-033).

REFERENCES

[1] P. S. Almeida, D. Camponogara, M. Dalla Costa, H. Braga, and J. M. Alonso, “Matching LED and driver life spans: a review of different techniques,” *IEEE Ind. Electron. Mag.*, Vol. 9, No. 2, pp. 36-47, Jun. 2015.

[2] X. Wu, C. Hu, J. Zhang, and Z. Qian, “Analysis and design considerations of LLCC resonant multioutput dc/dc LED driver with charge balancing and exchanging of secondary series resonant capacitors,” *IEEE Trans. Power Electron.*, Vol. 30, No. 2, pp. 780-789, Feb. 2015.

[3] Electromagnetic Compatibility (EMC)—Part 3-2: Limits for Harmonic Current Emissions (Equipment Input Current _16 A per Phase), Edition 2.1, IEC Standard 61000-3-2,

Oct. 2001.
[4] ENERGY STAR. (2008). *ENERGY STAR program requirements for solid state lighting luminaires. Eligibility criteria—Version 1.1* [Online]. Available:http://www.energystar.gov/ia/partners/product_specs/program_reqs/SSL_prog_req_V1.1.pdf
[5] E. Rifa, "Electrolytic capacitors application guide," Appl. Note, Evox Rifa AB, Gra¨nna, Sweden, 2001.
[6] U.S. Dept. Energy, "Lifetime of White LEDs, energy efficiency and renewable energy," Washington, DC, USA, Sep. 2009.
[7] H. Ma, C. Zheng, W. Yu, B. Gu, J.-S. Lai, and Q. Feng, "Bridgeless electrolytic capacitor-less valley-fill AC/DC converter for offline twin-bus light-emitting diode lighting application," *IET Power Electron.*, Vol. 6, No. 6, pp. 1132-1141, Jul. 2013.
[8] Y. C. Li and C. L. Chen, "A novel single-stage high-power-factor AC-to-DC LED driving circuit with leakage inductance energy recycling," *IEEE Trans. Ind. Electron.*, Vol. 59, No. 2, pp. 793-802, Feb. 2012.
[9] P. S. Almeida, H. A. C. Braga, M. A. Dalla Costa, and J. M. Alonso, "Offline soft-switched LED driver based on an integrated bridgeless boost–asymmetrical half-bridge converter," *IEEE Trans. Ind. Appl.*, Vol. 51, No. 1, pp. 761-769, Jan./Feb. 2015.
[10] M. Arias, M. Fernandez, J. E. Rodriguez, D. G. Lamar, and J. Sebastian, "Digital implementation of the feedforward loop of the asymmetrical halfbridge converter for LED lighting applications," in *Proc. IEEE Energy Convers. Congr. Expo*, pp. 3465-3472, Sep. 15-19, 2013.
[11] C. Branas, F. J. Azcondo, and R. Casanueva, "Feedforward compensation of resonant converters with heavy ripple in the DC bus for LED lamp driver applications," in *Proc. IEEE 14th Workshop Control Model. Power Electron*, pp. 1-6, Jun. 23-26, 2013.
[12] D. Camponogara, D. Ribeiro Vargas, M. A. Dalla Costa, J. M. Alonso, J. Garcia, and T. Marchesan, "Capacitance reduction with an optimized converter connection applied to LED drivers," *IEEE Trans. Ind. Electron.*, Vol. 62, No. 1, pp. 184-192, Jan. 2015.
[13] H. Broeck, G. Sauerlander, and M. Wendt, "Power driver topologies and control schemes for LEDs," in 2007-*Twenty second Annual IEEE Applied Power Electronics Conference* (*APEC*), pp. 1319-1325, 2007.
[14] Y. Ji, D. Jung, J. Kim, Y. Kim, and C. Won, "A phase lagging compensation for output current of DCM flyback based PV micro-inverters," in 2012 *7th International Power Electronics and Motion Control Conference*(*IPEMC*), pp. 1247-1251, 2012.
[15] G. Spiazzi, S. Buso, and G, Meneghesso, "Analysis of a high-power-factor electronic ballast for high brightness light emitting diodes," in *IEEE* 36*th Power Electronics Specialists Conference* (*PESC*), pp. 1494-1499, 2005.
[16] *Platinum DRAGON*R_ *Warm White With Chip Level Conversion*, OSRAM Tech.Datasheet 2D-93049 [Online].Available: http://www.osram-os.com
[17] *Luxeon LXK2 White LED.* (2006). Datasheet DS51. [Online]. Available: http://www.lumileds.com
[18] S. Buso, G. Spiazzi, M. Meneghini, and G. Meneghesso, "Performance degradation of high-brightness light emitting diodes under dc and pulsed bias," *IEEE Trans. Device Mater. Rel.*, Vol. 8, No. 2, pp. 312-322, Jun. 2008.
[19] P. T.Krein, "Current quality and performance tradeoffs under active power factor correction," in *Proc. IEEE Workshop Comput. Power Electron*, pp. 97-101, 2004.

Kai Yao was born in Jiangsu Province, China, in 1980. He received his B.S. degree in Industrial Automation from Nantong University, Nantong, China, in 2002; and his M.S. degree in Mechanical Design and Theory and his Ph.D. degree in Electrical Engineering from the Nanjing University of Aeronautics and Astronautics, Nanjing, China, in 2005 and 2010, respectively. In 2011, he joined the Faculty of Electrical Engineering, School of Automation, Nanjing University of Science and Technology, where he has been engaged in teaching and research in the field of power electronics. His current research interests include power factor correction converters, renewable energy generation systems and power supplies for LEDs.

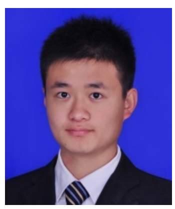

Xiaopeng Bi was born in Shandong Province, China, in 1990. He received his B.S. degree in Automation from Xiangtan University, Xiangtan, China, in 2013. He is presently working towards his M.S. degree in Power Electronics from the Nanjing University of Science and Technology, Nanjing, China. His current research interests include power factor correction converters and power supplies for LEDs.

Siwen Yang was born in Fujian Province, China, in 1992. He received his B.S. degree in Electrical Engineering and Automation from Jiangsu University, Zhenjiang, China, in 2015. He is presently working towards his M.S. degree in Power Electronics from the Nanjing University of Science and Technology, Nanjing, China. His current research interest include power factor correction converters.